Mechanism of Hook Formation in Ultralow-carbon Steel

Based on Microscopy Analysis and Thermal-stress Modeling

A new mechanism for the formation of hooks and oscillations marks during continuous casting of ultralow-carbon steels is presented. Previous experimental observations, plant data and theoretical modeling results are also considered.

Periodic transverse depressions, called "oscillation marks" (OM), are routinely observed on the surface of steel slabs manufactured by continuous casting processes.[1–3] Additionally, a distinctive subsurface microstructural feature called a "hook"[2,4–5] often accompanies deep oscillation marks in steels with low (< 0.1%) carbon contents.[4,6] Figure 1 shows typical shapes and sizes of oscillation marks and hooks observed on specially etched samples obtained from ultralow-carbon (0.003% C) steel slabs cast at POSCO Gwangyang Works, South Korea.[7–8] Hooks can be classified as "curved" (Figure 1a) if they angle steeply inward from the surface or "straight" (Figure 1b) if they are shallow and lie just beneath and parallel to the surface.[9] Curved hooks reach deeper beneath the surface (1.42 mm vs. 0.48 mm for straight hooks) and are accompanied by deeper oscillation marks (0.26 mm vs. 0.19 mm for straight hooks). Each hook has a central line, the "line of hook origin," which distinguishes the region inside the hook microstructure from the portion that solidified after liquid steel overflow.

Severe hook and oscillation mark formation degrade the slab surface quality, owing to the entrapment of argon bubbles and alumina inclusions near the hook,[10–11] and the formation of transverse cracks near the roots of oscillation marks.[1,3,6] Transverse cracks initiate due to the coarser grain structure and presence of embrittling precipitates often found in this region.[3,6] In extreme cases, the entire slab surface must be ground or "scarfed" to completely remove these defects, resulting in loss of productivity.[7]

The formation of hooks and oscillation marks is associated with vertical oscillation of the water-cooled copper mold, which significantly alters the local heat transfer, fluid flow and initial solidification in the meniscus region. The oscillation is required to facilitate smooth withdrawal of the solidifying steel shell from the mold by preventing the shell from sticking to the mold wall. This is aided by a "negative strip time" period during the cycle, when the mold moves downward faster than the casting speed. Oscillation also pumps molten flux into the gap formed between the shell and mold faces, where it acts as a lubricant. The flux is added as a powder to the top free surface of the liquid steel pool. It melts to create a continuous liquid flux layer that conforms to the steel surface contour and flow field, and provides thermal and chemical insulation to the liquid steel. In addition to the mold oscillation frequency and stroke, many different parameters affect oscillation mark formation, including the casting speed, superheat temperature difference and liquid steel flow pattern in the mold.

Several studies focusing on low-, medium- and high-carbon steels have been conducted in the past to explain hook and oscillation

Authors

Joydeep Sengupta (top left), research leader, Dofasco Inc., Hamilton, Ont., Canada (joydeep_sengupta@dofasco.ca); **Brian G. Thomas** (top right), Wilkins professor, University of Illinois at Urbana-Champaign, Urbana, Ill. (bgthomas@uiuc.edu); **Ho-Jung Shin** (bottom left), researcher, POSCO Technical Research Laboratories, Gwangyang, South Korea (ceraby@posco.com); and **Seon-Hyo Kim** (bottom right), professor, Pohang University of Science and Technology, Pohang, South Korea (seonhyo@postech.ac.kr)

Figure 1

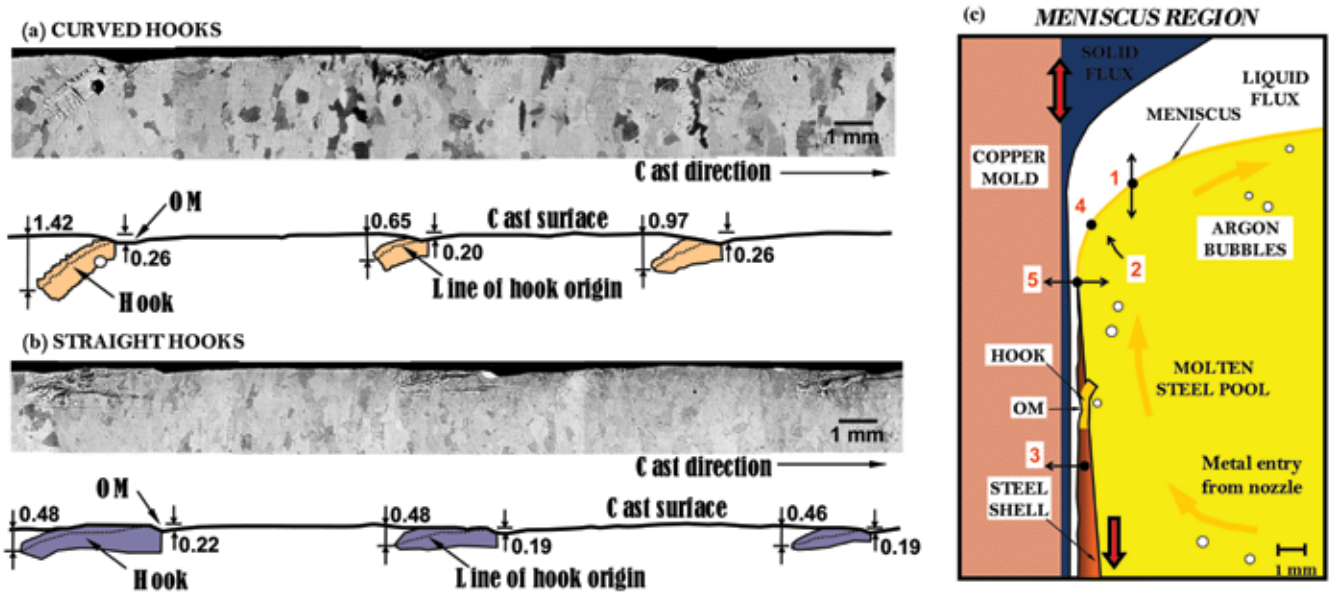

Three consecutive oscillation marks accompanied by (a) curved and (b) straight hooks observed on ultralow-carbon steel slabs[7–8]; and (c) complex phenomena occurring inside a continuous caster mold influence initial solidification in the meniscus region.

mark formation, which is crucial to optimizing casting conditions and improving the process. Most of the mechanisms proposed so far are based on transient events occurring near the meniscus, which involve a range of complex, interrelated phenomena illustrated in Figure 1c:

1. Pressure fluctuations in the liquid flux channel dynamically alter the meniscus shape.
2. The turbulent flow pattern in the mold cavity brings liquid to the meniscus region with varying amounts of superheat.
3. Heat is conducted from the solidification front to the mold through the steel shell and the interfacial gap, which consists of liquid and re-solidified layers of mold flux.
4. The meniscus region might solidify, depending on the local superheat of the liquid, the availability of nucleation sites, the ease of nucleation and growth, and alloy properties such as freezing range.
5. The mold or slag rim may interact with the shell during the negative strip period, especially if mold friction is large enough to generate significant axial stresses and deformation. Rapid changes in temperature gradient may cause thermal distortion of the shell tip, depending on the mechanical properties of the steel grade.

All the above events are expected to alter the rate of solidification near the meniscus and ultimately dictate the shape and size of subsurface hooks and oscillation marks. However, these mechanisms offer conflicting explanations, and are often speculative and incomplete. For example, there is no agreement on when hooks form during the oscillation cycle or if they form by: (a) bending of the initial shell tip[12–13] or (b) freezing of the liquid steel meniscus.[2,4,14–16] Similarly, wide differences exist between mechanisms proposed for oscillation marks and surface depressions, which include: (a) healing of disjointed steel shell edges,[17–19] (b) mechanical interaction between the mold and shell,[20] (c) shell bending[12–13] and (d) thermal distortion,[21] followed by liquid overflow over the shell tip and subsequent solidification.

A major impediment toward developing a robust understanding of initial solidification is the difficulty of observing hooks in cast samples. Special grade-specific etching reagents[4,6,22] are required to clearly reveal the initially solidified structure near the hook, prior to subsequent phase transformations. Previous efforts to observe hook features on slab samples have used either picric acid solution[3,12] or Oberhoffer's reagent.[3] Although picric acid solution reveals the dendritic structure close to the oscillation mark, the hook is difficult to distinguish from the rest of the microstructure. On the other hand, Oberhoffer's reagent relies on the segregation of phosphorus, and can reveal only the linear profile of a hook, but not the dendritic structure close to it. Thus, better etching reagents are needed. Furthermore, the relationship between the dendrite/hook microstructure

Table 1

Details of Casting Parameters for Slab Samples Obtained From POSCO

Micrograph analysis presented in:	Slab width (mm)	Pour temperature (°C)	Casting speed (mm/s)	Mold oscillation frequency (Hz)	Mold oscillation stroke (mm)
Figures 2 and 4	1,300	1,564	28.2	3.02	6.19
Figure 3	1,300	1,565	28.2	3.02	6.18
Figure 5	1,960	~1,565	~16.7	1.90	5.67

and the final solidified grain structure has not been investigated in previous work. Scanning electron microscopy has also not been exploited to study hook formation.

Although microstructural analysis may provide important new information, it cannot reveal the detailed steps that lead to the final microstructure and morphology. Therefore, fundamentally based comprehensive mathematical models are required to predict events leading to hook and oscillation mark formation; but this is indeed a daunting task, requiring fully coupled, transient thermal,fluid-flow and stress analysis. To date, very few mathematical models have been applied to understand initial solidification phenomena in the mold cavity and investigate surface defect formation. The uncoupled thermal-mechanical model of shell tip bending by Schwerdtfeger and Sha[13] predicted inward tip bending up to ~0.6 mm, but the predicted oscillation mark depth did not decrease with higher mold oscillation frequencies and casting speeds, as observed in industry. The coupled thermal-stress model by Thomas and Zhu[21] predicted a shell tip deflection of ~1.65 mm for a liquid level drop of 20 mm for 1.2 seconds, which rarely occurs; hence, this mechanism alone cannot explain the deep hooks (up to ~2 mm) observed in every one of a series of oscillation marks in an ultralow-carbon steel slab cast at POSCO (Figure 1b).

To address the above issues, the present study was conducted to reveal new information about hook formation in ultralow-carbon steels. Both optical and scanning electron microscopy were performed to simultaneously distinguish the hook structure, the surrounding dendrite microstructure, the final grain structure, the grain orientations relative to the hook, and the local composition variations. This study also describes the application of a transient thermomechanical model to compute temperature, stress development, and distortion of a steel shell during the initial stages of solidification by considering the effect of sudden metal level fluctuations at the meniscus. The model is based on a well-validated transient thermal-elastic-viscoplastic finite element (FE) code, CON2D,[23] available at the University of Illinois at Urbana-Champaign, and builds on previous work by Thomas and Zhu.[21] The results obtained from these different sources reveal unique insights into hook and oscillation mark formation during the initial stages of solidification in the meniscus region for ultralow-carbon steels.

Experimental Methods

An experimental campaign was conducted on a conventional continuous slab caster, No. 2-1, at POSCO Gwangyang Works, South Korea, which features a standard 2-port submerged entry nozzle and a 230-mm-thick parallel mold with a fully adjustable, nonsinusoidal hydraulic oscillator. Electromagnetic current was employed to control fluid flow conditions in the liquid pool. Table 1 summarizes the casting parameters employed to obtain the various slab samples from the caster for this study. Further details are given elsewhere.[7–8]

The composition of the ultralow-carbon steel grade used during the trials was: Fe with 0.003% C, 0.08% Mn, 0.005% Si, 0.015% P, 0.01% S, 0.01% Cr, 0.01% Ni, 0.01% Cu, 0.05% Ti and 0.04% Al. The liquidus and solidus temperatures of this steel grade are 1,533°C and 1,517°C, respectively. The mold powder contained: 39.8% CaO, 36.33% SiO_2, 6.72% F, 5.97% Al_2O_3, 3.43% Na_2O, 0.84% MgO, 0.35% Li_2O, 0.34% Fe_2O_3, 0.18% TiO_2, 0.11% K_2O, 0.03% MnO_2, 1.97% free C and 3.01% total C. Its melting temperature is 1,145°C, and viscosity at 1,300°C is 2.62 Poise.

Samples (100 mm long and encompassing ~10–12 oscillation marks) were obtained near the surface of the narrow faces of 1,300-mm-wide slabs at five different distances between the wide faces. Sections through each sample were cut, mechanically ground and polished to ~0.25 μm. These were then etched by picric acid solution with additions of the cationic surface-active reagent or "surfactant"[24] zephiramine (Benzyldimethyl-n tetradecylammonium chloride) for ~1–1.5 hours. The etching reagent was identified by conducting an intensive experimental program at Postech to reveal the solidification microstructure and delineate the hook features in this difficult-to-etch steel grade with ultralow alloy content under an optical microscope. Thus,

Figure 2

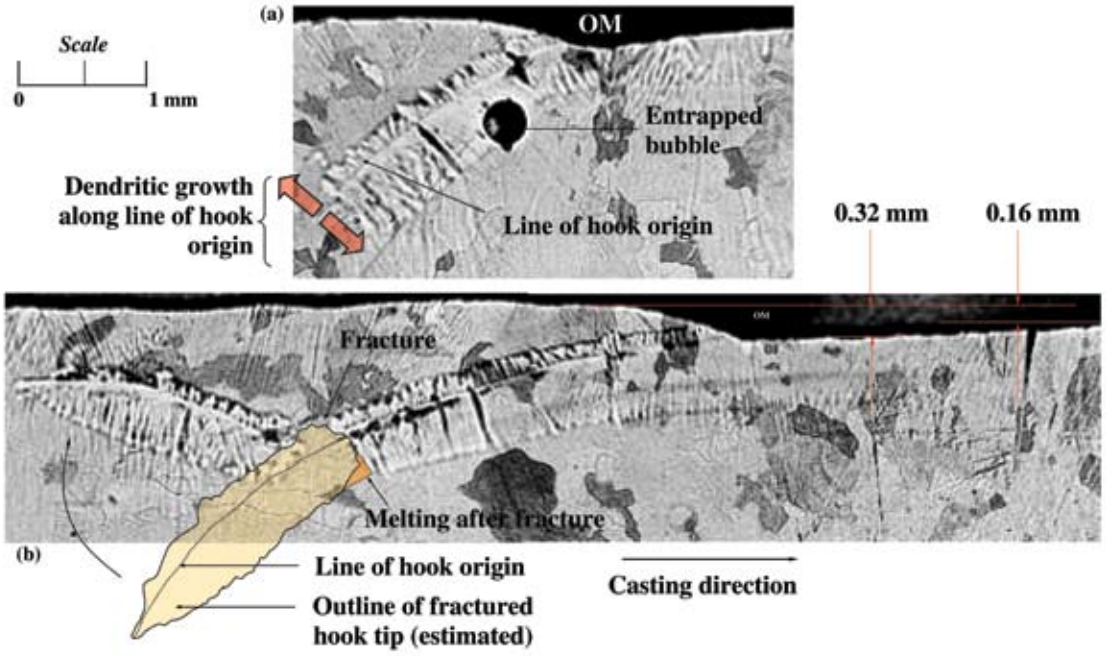

Hook features in ultralow-carbon steel samples: optical micrographs showing (a) entrapment of argon bubble by a hook-type oscillation mark and (b) a fractured hook tip.

micrographs (or two-dimensional vertical section views) were obtained from each three-dimensional hook structure[25] and oscillation mark at different locations on the narrow face. The shape of these three-dimensional structures does not vary much with distance along the slab perimeter. Near the corners of the slab, however, the hooks exhibit complex three-dimensional shapes, but metallographic analysis of these effects is beyond the scope of this study.

The distribution of crystallographic orientation in the microstructure near the hook region was analyzed by the electron backscattering diffraction (EBSD) method using a JEOL JSM-7000F® field emission analytical scanning electron microscope. The microscope was equipped with an HKL Technology® EBSD system with a high-resolution (up to 1.2 nm for a 30-kV accelerating voltage) detector that allowed accurate analysis of Kikuchi patterns over an area of 300 µm x 400 µm in steps of 2 µm. The samples were first electropolished by a 95% acetic acid-5% perchloric acid solution with a current of 0.2 A for 60 seconds. The data obtained from EBSD was analyzed using the HKL Technology Channel 5® suite of programs, which can display subtle changes in orientation along a line running across grains or subgrains. The hook region of samples from a 1,960-mm-wide slab was also subjected to elemental analysis by the energy-dispersive x-ray spectroscopy (EDXS) method using a JEOL JSM-59® scanning electron microscope.

Metallographic Assessment of Hook Shapes — Figure 2a shows a typical curved hook adjacent to an oscillation mark in one of the slab samples, shown in Figure 1b. Each hook has a curved line, determined to be the line of hook origin, which indicates the shape of the meniscus after it solidified. Groups of dendrites growing both away from and toward the mold surface from this line can be clearly distinguished, owing to the marked improvement of the current etching method over those used in previous studies.[3,12] The characteristic features (e.g., length, depth and thickness) of the hook can be easily measured from the micrograph. Traces of entrapped argon bubbles and inclusion particles were often found in the vicinity of curved hooks, such as can be seen in Figure 2a. The perpendicular distance from the slab surface to the furthest inner extent of the hook indicates the thickness of surface layer that has to be removed to eliminate the hook and the entrapped bubble.

Figure 2b shows a different curved hook located 35 mm (three OMs away) from the hook in Figure 2a. This micrograph illustrates that a portion of the hook can be separated from the solidified meniscus. This indicates brittle fracture (hot tearing) of the fragile semi-solid hook that was likely caused by inertial forces of the molten steel acting during its overflow of the curved hook. This hypothesis is confirmed by the fact that the edges of the outline (estimated initial position) of the separated hook tip and the fractured hook in the figure align almost exactly. Just a

small portion of the bottom edge of the hook tip is missing, which appears to have been melted away by the flowing liquid steel. The rest of the hook tip floated away and became entrapped in the solidifying shell growing above the hook. Usually, the fractured shell tip completely melts or is transported away, giving rise to the truncated end observed in most hooks, including the one in Figure 2a.

The etched hook sample in Figure 3 clearly reveals dendrites originating from several different nucleation sites located on or near the frozen meniscus (i.e., line of hook origin). Some dendrites grew away from the mold wall. Others grew into the liquid overflow region toward the mold wall, stopped growing and coarsened. The rest of the overflowed region solidified later, producing a finer structure, as heat was rapidly removed into the mold wall. A group of dendrites growing toward the molten steel abruptly changed direction near the truncated edge, in contrast to the uninterrupted growth in the same direction nearer to the base of the hook. This observation suggests that the truncated hook tip moved when liquid steel overflowed. If meniscus solidification and overflow occur during the negative strip period,[26–27] it is proposed that the positive pressure in the flux channel can break the hook tip and rotate it slightly.

Figure 3

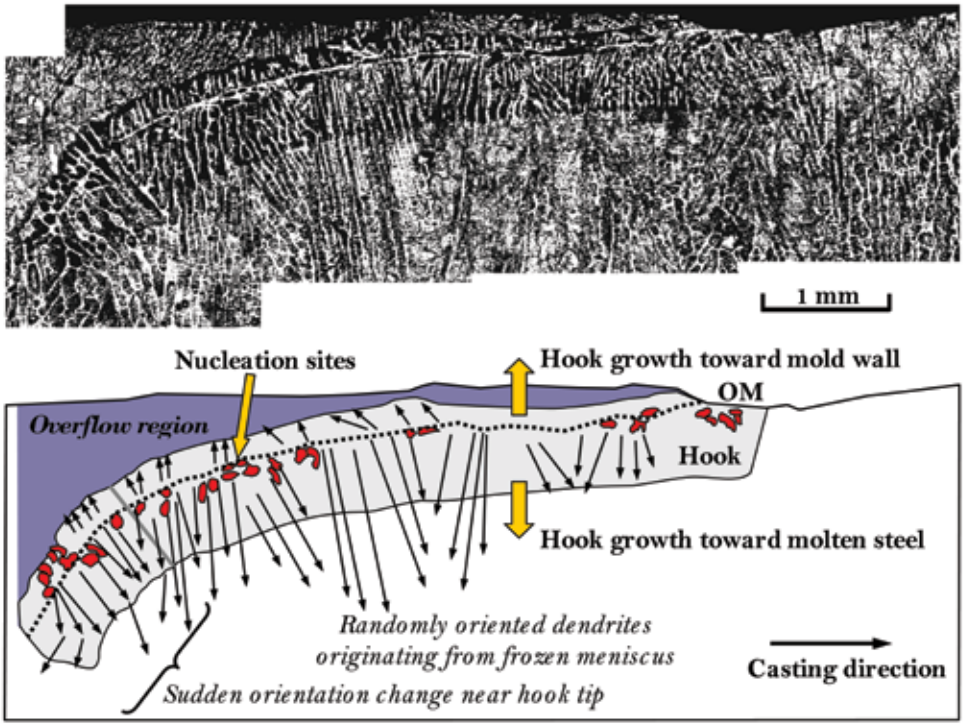

Optical micrograph of an ultralow-carbon steel sample showing unidirectional growth of dendrites originating from nucleation sites located at the line of hook origin (or frozen meniscus).

Orientation of Grains Near the Hook Region — Figure 4 shows an EBSD map of crystallographic orientations (left) obtained from an area near the line of hook origin on the slab sample shown in Figure 2a. The location of this area relative to the hook is also indicated on a backscattered electron SEM image (right). As an SEM image does not reveal the hook features without etching, the actual hook shape was traced from Figure 2a and transferred to this image. Grain misorientation plots were obtained along lines (such as "a-b" indicated in the figure) running across the grains in the microstructure. By combining the results measured along four different lines, grain misorientations for all the grains ("B" through "F") relative to the largest grain ("A") were calculated and indicated on the map. It can be clearly seen that the grains below the solid black line have higher relative misorientation than the grains above this line, which is a long grain boundary. The SEM image clearly shows that this line is indeed also a short segment of the line of hook origin. The drastic difference in relative grain orientations can be explained by the fact that solidification above and below the line of hook origin occurred at different

Figure 4

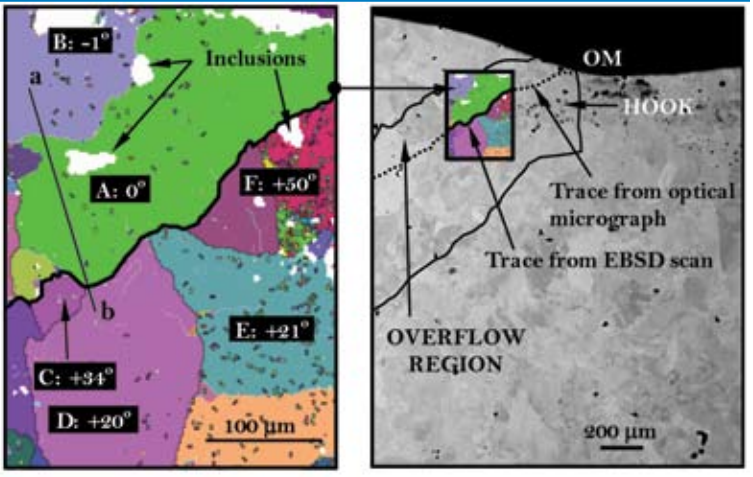

Electron backscatter diffraction map (left) of grain misorientation measured near the hook shown in Figure 1a, and distant view (EBS image) (right) showing location relative to line of hook origin.

Figure 5

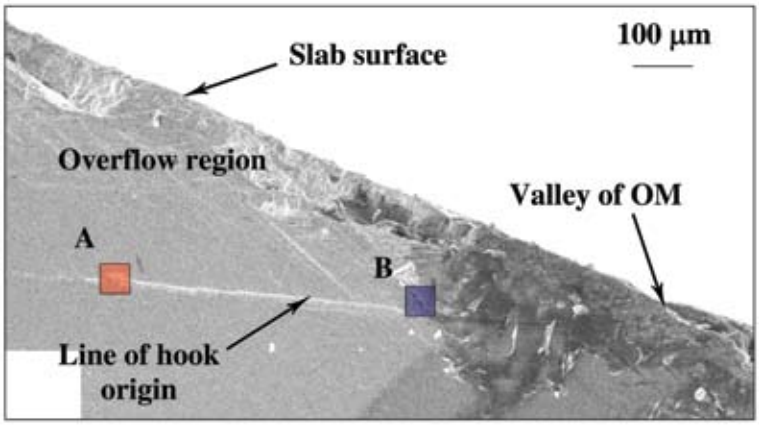

Element	Area A (wt %)	Area B (wt %)
C	5.65	16.6
S	0.22	—
Mn	0.68	—
F	0.81	—
O	—	47.16
Ca	—	33.11
Fe	Bal.	Bal.

Energy dispersive x-ray spectroscopy (EDXS) analysis at two locations on the line of hook origin shown on the SEM image reveals traces of fluorine and calcium oxide, which are present in the mold powder but not in the ultralow-carbon steel.

times during the oscillation cycle. First, the lower region solidified while the interface (meniscus) was covered with mold flux, and then the upper side solidified during subsequent liquid steel overflow.

Elemental Analysis of the Hook Region — EDXS analysis was conducted at two regions along the line of hook origin indicated on the SEM image shown in Figure 5. Traces of fluorine and calcium were detected at areas "A" and "B," respectively. Since these elements are absent in the steel grade being investigated but are present in the mold powder, the appearance of these foreign elements along the line of hook origin can be explained only if the molten flux was retained by the δ-ferrite dendrites growing along the frozen meniscus, prior to liquid steel overflow. Clearly, some mold flux was entrapped by the overflow of liquid steel over the line of hook origin as solidification proceeded rapidly toward the mold wall. The authors believe that the surfactant used in the etching reagent preferentially reacted with the elements present in the mold powder that penetrated between the dendrites, and thus enabled the shape of the hooks and

Figure 6

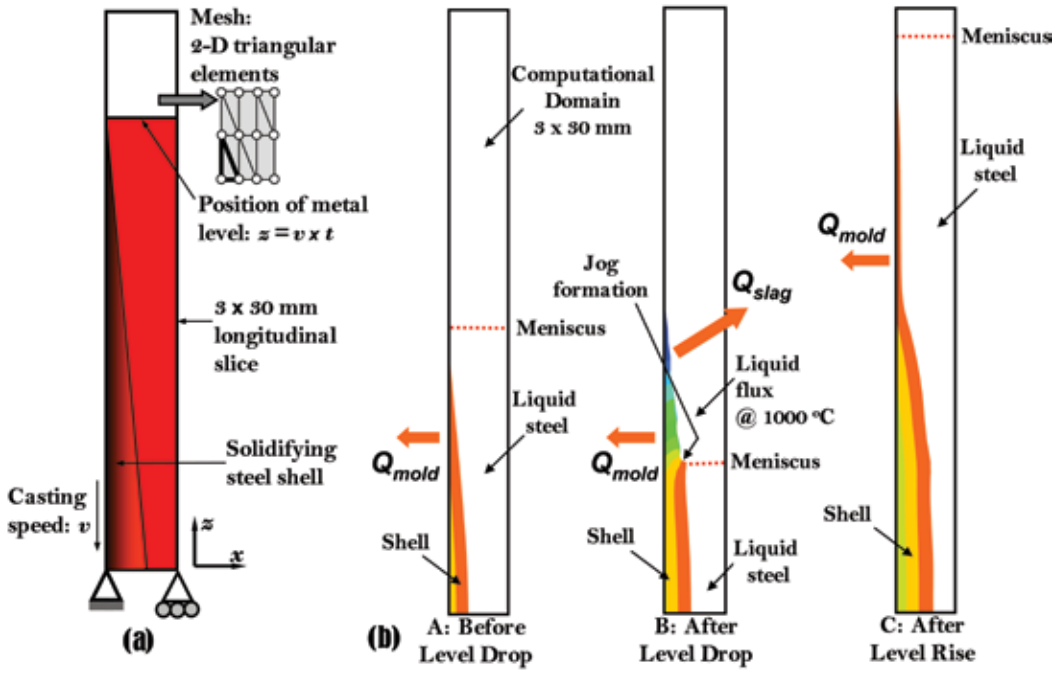

(a) Computational domain and mechanical boundary conditions used in CON2D for predicting shell distortion due to a sudden level fluctuation event, and (b) thermal boundary conditions for the three different stages of the event.

Figure 7

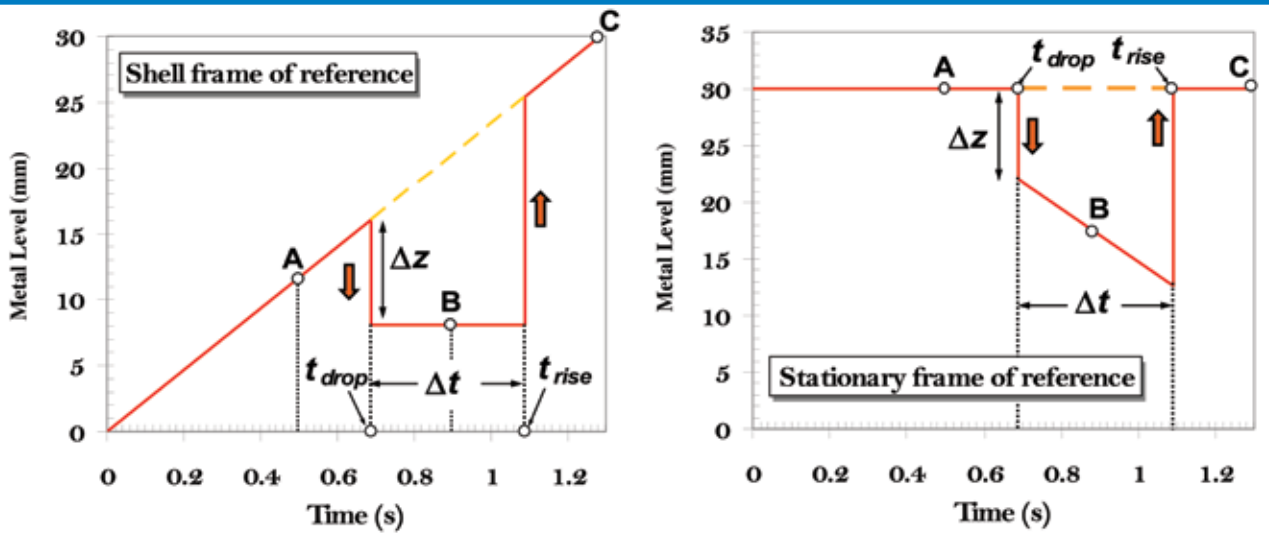

Position of metal level inside the computation domain during a level fluctuation event in the (a) moving (attached to shell) and (b) stationary frames of reference. A, B and C are three specific instants during the level fluctuation event — i.e., before level drop, after level drop and after level rise, respectively.

the fractured hook tip in Figure 2b to be revealed by optical microscopy.

Finite Element Modeling Methodology — The finite element (FE) model simulates the thermomechanical behavior of a solidifying ultralow-carbon steel shell, as it moves down the 230-mm-thick parallel mold at a casting speed (v) of 23.33 mm/second or 1.4 m/minute. The liquidus and solidus temperatures of this steel grade are 1,533°C and 1,517°C, respectively. The mold oscillation frequency and stroke are 2.58 Hz or 155 cpm and 6.34 mm, respectively. These casting parameters correspond to typical operating practice at POSCO. Figure 6a shows the computational domain, which is a 3 mm x 30 mm longitudinal slice along the centerline of the wide face (1,300 mm in length) near the meniscus.

The longitudinal slice enters the mold and moves downward at the casting speed. Solidification proceeds from the left edge of the domain. At any time t, the metal level (ignoring meniscus curvature) is located just above the shell tip at $z = v \cdot t$ mm (see Figure 6a). Then, a sudden drop in metal level (by Δh mm) at t_{drop} = 0.69 second is imposed, exposing the inner edge of the shell to the liquid flux layer that floats above the liquid steel. Finally, a subsequent level rise occurs at t_{rise} = 1.09 seconds. The duration of the level fluctuation, Δt = 0.4 second, corresponds to an oscillation cycle, or a chaotic wave generated by the turbulent flow. Figures 7a and b track the metal level changes in moving and stationary frames of reference, respectively, which are used to simulate a single level fluctuation event.

The heat flow model solves the two-dimensional transient energy equation, using a fixed Lagrangian grid of 3-node triangles. Temperature-dependent thermal conductivity and enthalpy functions are used to incorporate the effects of solidification and solid-state phase transformation on the heat flow across the domain.[23] A nonequilibrium microsegregation model incorporating the effects of several alloying elements is used to calculate the liquidus, solidus and peritectic temperatures, and phase fractions.[28] Within each time step, temperatures are first computed by the heat transfer model. After interpolating the thermal loads onto a fixed-grid finite element mesh of 6-node triangles, the stress model then solves for stresses, strains and displacements. The effects of stiffness and volume changes during solidification are incorporated through temperature-dependent Young's modulus and thermal linear expansion functions.[23]

To discretize the computational domain, a grid size of 31 nodes x 61 nodes (mesh resolution: 0.1 mm x 0.5 mm) was selected based on a sensitivity analysis conducted for a normal solidification case without any level fluctuation. The computational domain is initially assumed to contain stress-free liquid at a uniform temperature, corresponding to a pour temperature of 1,565°C employed during the casting process. Solidification within the domain is achieved by imposing a Cauchy-type heat transfer boundary condition on the left edge corresponding to the heat flow toward the water-cooled mold. However, a zero heat flux boundary condition is imposed on a portion of the left edge located above the metal level.

The heat flux (Q_{mold} in W/m^2) boundary condition corresponding to mold (or primary) cooling before the level drop (event "A" in Figure 6b) is given by:

Figure 8

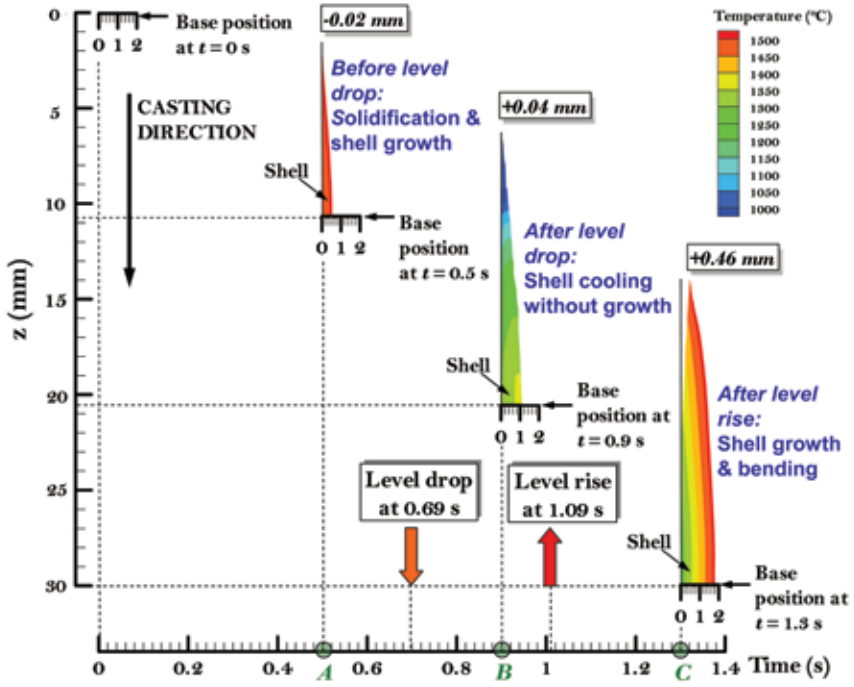

Evolution of temperature field and shell tip deformation during a level fluctuation event. Plots for three representative times are shown: (A) 0.19 second before the level drops, (B) 0.21 second after the level drops and (C) 0.21 second after the level rises again.

$$Q_{mold} = 0$$

for t > 0 s, $x = 0$ mm and $z > z = v \cdot t$ (Eq. 1)

$$Q_{mold} = h_{mold} (T - T_{mold})$$

for t > 0 s, $x = 0$ mm and $z \leq z = v \cdot t$ (Eq. 2)

The mold wall is assumed to be at a constant (sink) temperature of T_{mold} = 250°C, and the heat transfer coefficient, h_{mold} of 4,000 W/m^2–K (corresponding to a heat flux of ~5.0 MW/m^2 near the meniscus) is used in the heat flow model. Zero heat flux is assumed across the top, bottom and the liquid steel sides of the domain.

At time t_{drop} = 0.69 second, the level drops suddenly by ~16 mm (event "B" in Figure 6b) for a duration of 0.4 second. During this time, the thermal conductivity and specific heat of the nodes in the liquid steel region (beyond the solidification front) are artificially lowered to simulate the entrance of liquid flux at a constant temperature of T_{flux} = 1,000°C in the domain to replace the liquid steel. The following boundary condition is imposed along the exposed solid shell, defined by the location of the solidus isotherm at the time of the level drop:

$$Q_{flux} = h_{flux} (T - T_{flux})$$

for $t_{drop} \leq t \leq t_{rise}$ with h_{flux} = 1,500 W/m^2–K (Eq. 3)

Finally, the level is raised again at time t_{rise} = 1.09 seconds (event "C" in Figure 6b) by restoring the liquid elements at the initial temperature, and allowing solidification to proceed normally. Since the level is restored above the shell tip, the model simulates meniscus overflow, which is an important event associated with oscillation mark formation.[2,12–13] The model ignores nonuniform dissipation of superheat and nucleation undercooling near the meniscus; hence, the possibility of meniscus solidification is not considered.

The mechanical boundary conditions imposed on the domain are indicated in Figure 6a. The shell tip is free to move away from or toward the mold so that the formation of an oscillation mark or a surface depression can be simulated. Rigid body motion in the domain is prevented by fixing three nodal displacements of the bottom-left node and by preventing the movement of the bottom edge along the casting direction. Mold friction and pressure forces imposed on the shell by the liquid flux and slag rim (~1 kPa), and ferrostatic pressure (~0.002 MPa at the bottom of the domain) are ignored. Although these effects are important to meniscus shape, they are not expected to affect the distortion of the solid shell caused by thermal stress. The longitudinal slice is assumed to remain planar as it moves down the mold; thus, the stress state in the wide and thin shell follows a generalized plane strain mode, allowing the two-dimensional model to reasonably estimate a complete three-dimensional stress state for the domain under consideration.

Model Predictions — Figure 8 shows the evolution of shell shape and distortion at three different times during the level fluctuation event (refer to Figure 7) computed by the model as the domain traverses the mold length consistent with the casting speed. The stresses across the thickness (σ_{xx}) and in the transverse direction (σ_{yy}) are very small (< ± 1.0 MPa) for a shell length of ~16 mm owing to rapid creep relaxation and low elastic modulus at high temperatures. Referring to the figure, it can be seen that, before the level drop event, solidification dictated by heat flow toward the mold proceeds with time and a thermal gradient quickly develops inside the shell. The surface cools rapidly, causing the shell tip to bend toward the mold (by ~0.02 mm) and axial tensile stress to develop near the surface.

Figure 9

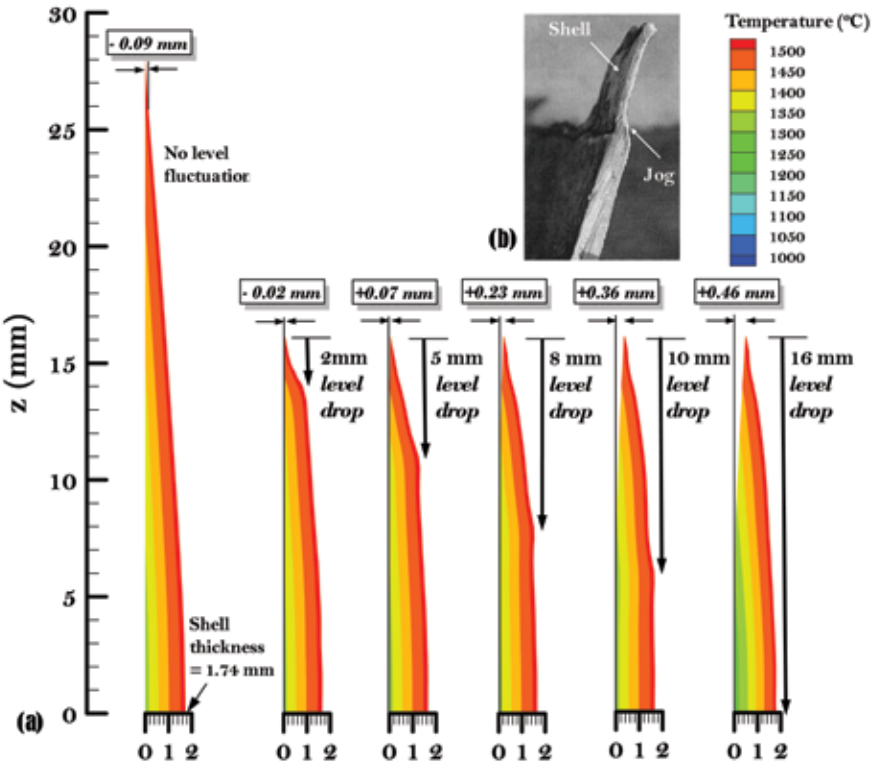

(a) Comparison between shell distortion predictions for different magnitudes of level drop and normal solidification (no level fluctuation); and (b) jog formation on the inside edge of the shell observed by Fredriksson and Elsberg[30] in a breakout shell.

After the level drops, exposing the shell to mold flux, the shell temperature decreases rapidly (~200°C in 0.19 second) because the mold extracts sensible heat from the thin shell very quickly in the absence of heat supply from the liquid steel. The thermal gradient inside the shell also disappears, causing the shell interior to contract more than its exterior. Thus, a relatively large compressive stress develops at the surface, and the shell tip bends away from the mold wall (by ~0.04 mm). Suddenly raising the liquid level back up to the shell tip is predicted to rapidly increase the shell temperature, shell thickness and distortion. Liquid steel comes in direct contact with the colder shell, and a new skin grows over the older shell. Restoring the high-temperature gradient across the entire thickness tends to cause the older shell to expand. Because this is constrained by the newly solidified layer, the net effect is to bend the shell tip substantially toward the liquid steel (up to 0.46 mm within a 0.21-second time span).

Although a level drop of ~16 mm was chosen in the previous case to demonstrate the thermomechanical behavior of the shell during a level fluctuation event, a level drop of this magnitude occurs only rarely in an industrial casting machine, and is normally within ±10 mm.[29] Thus, the model was utilized to compute the shell shapes and distortions for smaller level fluctuations, keeping the duration constant at 0.4 second. The results are summarized in Figure 9a, which indicates that shell tip distortion is almost negligible for fluctuations below ~5 mm. An irregularity in the profile of the inner shell edge was always observed near the location where the liquid level remains stationary for 0.4 second during the level drop event. Ordinary solidification below this location increases the shell thickness, in contrast to the shell edge above this location, which does not grow due to the absence of liquid steel. Thus, the formation of a "jog" (refer to Figure 6b) is predicted by the model, similar to the one observed in the plant sample[30] in Figure 9b. This jog is smoothed out after the liquid level rise.

Implications for Hook and Oscillation Mark Formation

Figure 10a compares the lines of hook origin (dotted lines) obtained from successive hooks that were observed on a two ~100-mm-long steel slab samples obtained from POSCO. There is a wide variation of hook depth and length, indicating that hook formation is a complex event dictated by the time-dependent meniscus shape as it freezes over the initial shell tip. This observation shows that the shape of the meniscus can be significantly altered during the casting process. This can be attributed to: (a) periodic pressure forces generated in the flux channel by the oscillating mold[12,31] and (b) sudden localized metal level fluctuations initiated by chaotic turbulent motion in the molten pool or by abrupt changes in operating conditions.

The lines of hook origin in Figure 10a are compared with the "no-force" or equilibrium shape of the meniscus, determined solely by the balance of surface tension and ferrostatic pressure forces given by Bikerman's equation.[30] In calculating the predicted shape, a surface tension of 1.6 N/m was chosen, corresponding to the sulfur content of 0.01% for the steel grade,[32] and the steel density was assumed be 7,000 kg/m^3 at 1,560°C.[33] A reasonable match between the hook shapes and the shape predicted by Bikerman's equation confirms that curved hooks are indeed initiated by meniscus solidification in ultralow-carbon steel slabs. The figure shows that these hooks are curved much more than the maximum curvature expected from thermal distortion of the initial shell, even for a level

Figure 10

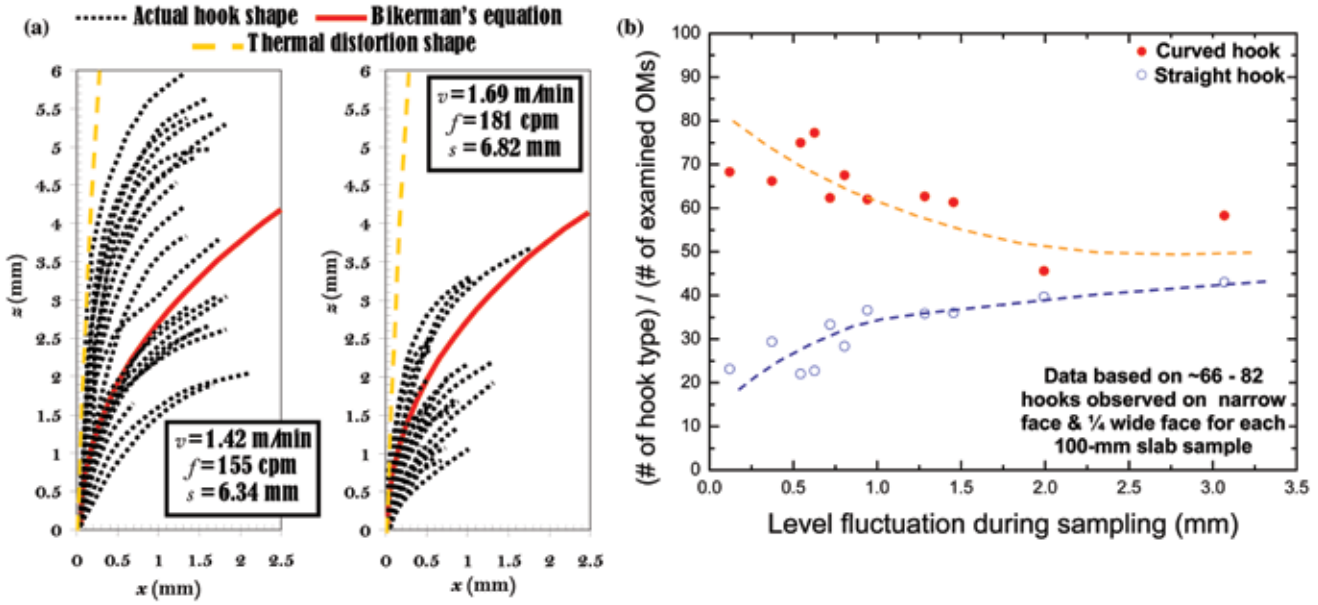

(a) Line of hook origin for successive hooks on slab samples cast at POSCO under two different conditions. Comparison with Bikerman's equation and predicted shell shape after a level fluctuation is also included; (b) occurrence of surface hooks increases with an increase in metal level fluctuation recorded during the casting process.

fluctuation of 16 mm for 0.4 second (obtained from Figure 9a). However, the shape of the bottom portion of the straight hooks (located close to the surface) may be caused by the thermal distortion effect after level fluctuations. This effect appears to play a greater role in the formation of straight hooks, as the occurrence of these hooks increases with level fluctuations during the casting process, as seen from Figure 10b.

Simultaneous analysis of the results revealed new information relating to hook formation in ultralow-carbon steel. These are summarized as follows:

- Formation of curved hooks is initiated by meniscus solidification. The instantaneous shape of the meniscus at this instant dictates the curvature of the line of hook origin. Recent work has established that this event usually occurs at the beginning of the negative strip period.[34] This is schematically illustrated in Figure 11a. In contrast, it is likely that straight hooks are initiated by thermal distortion of the shell tip, thus resulting in a smaller hook depth.
- The hook thickness below the line of hook origin is created by dendritic growth toward the molten steel, originating from nucleation sites along the line of hook origin (the meniscus).
- Some of the molten flux contacts the meniscus (line of hook origin) and penetrates between the dendrites of the solidifying hook,[25] where it is retained and revealed during etching.
- The meniscus subsequently overflows the line of hook origin during negative strip time[34] as soon as inertial forces in the fluid instantaneously exceed surface tension forces, as shown in Figure 11b. Dendrites quickly grow above the line of hook origin toward the mold wall into the overflowed liquid. The growth stops eventually as the meniscus region gains superheat. The hook edges are established as the dendrites coarsen due to the long local solidification time.[34] This event explains the sharp drop in the distance between solidified shell and mold wall during the negative strip time measured by Tsutsumi et al.[35] while observing oscillation marks and mold powder infiltration in a Sn-Pb alloy (metal) and stearic acid (flux) system. It also explains the rapid rise of mold heat flux throughout the negative strip time, observed during experiments by Badri et al.[26,36]
- The heavier liquid steel displaces liquid mold flux as it overflows. It also melts through some of the solid mold flux layer, bringing liquid steel closer to the mold wall. This explains the eventual outward bulge usually observed above every oscillation mark and line of hook origin. For example, in Figure 2b, the slab surface above the oscillation mark extends d = 0.32 mm beyond the oscillation mark root and 0.16 mm beyond the slab surface below the oscillation mark. This indicates that the overflow

Figure 11

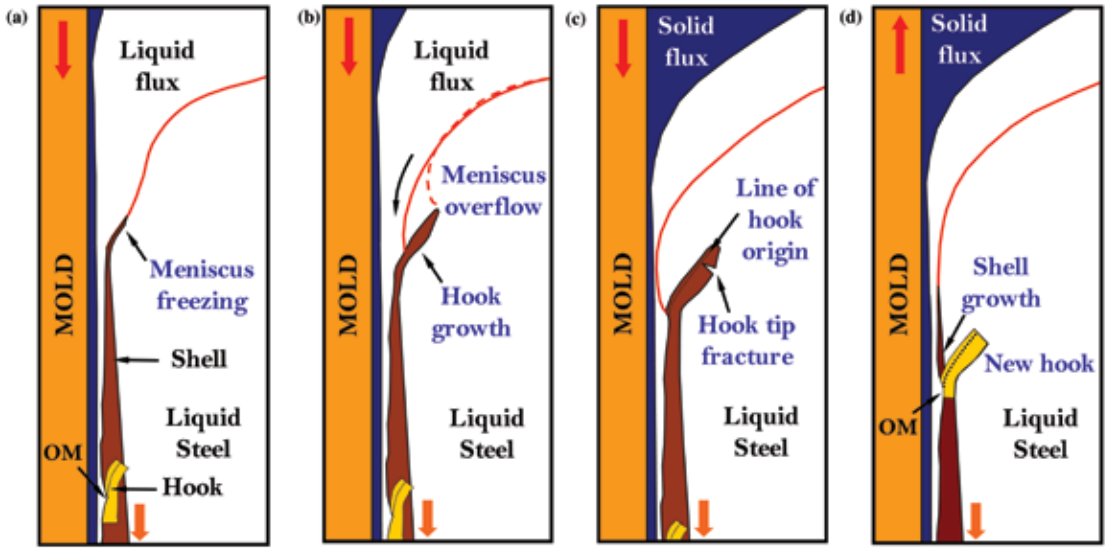

Schematics illustrating formation of curved hook in an ultralow-carbon steel slab by meniscus solidification and subsequent liquid steel overflow. Oscillation marks (OM) are formed by normal steel shell growth after overflow.

caused ~0.16 mm of the flux layer thickness to remelt.

- The heat transfer rate increases during this time because it is controlled by the gradually decreasing thickness of the mold flux layer that separates the mold and the molten steel. The heat transfer rate is largest while the steel is still liquid, before solidification produces a surface roughness and solid layer that slows down heat transfer.
- Molten flux is retained along the line of hook origin, which is revealed by EDS and EPMA analysis. Some flux is also retained within the overflowed region.
- The line of hook origin persists as grain boundaries in the final microstructure,[25] despite the occurrence of two separate phase transformations, as revealed by the EBSD analysis. Grains above and below the line of hook origin have distinctly different crystallographic orientations due to the temporal separation between meniscus freezing and liquid overflow.
- The final shape of the hook is completed as the hook tip fractures off and is carried away, as shown in Figure 11c.
- The overflow region solidifies forming the oscillation mark during the positive strip time. The extent of penetration of liquid steel into the flux channel determines the final shape of the upper side of the oscillation mark. The extra volume of flux entrapped in the oscillation mark during its formation at this time explains the sudden rise in tracer velocity measured in the stearic acid flux channel between the mold wall and shell during the positive strip time.[35] The hook protruding from the solidifying shell captures inclusions and bubbles in the liquid steel until the shell finally solidifies past the hook. These events are illustrated in Figure 11d.

Conclusions

The subsurface microstructure of continuous-cast, ultralow-carbon steel slabs has been examined using both optical microscopy and scanning electron microscopy using EBSD and EDX techniques. Careful selection of an etching reagent allowed the dendrites forming the hook to be clearly distinguished from the rest of the microstructure using optical microscopy. Measured shapes of the line of hook origin matched reasonably well with Bikerman's equation for meniscus shape. This confirms that periodic meniscus solidification during the continuous casting process causes curved hook formation.

Grain orientation measurements and elemental maps revealed that dendritic growth above the line of hook origin occurs after meniscus overflow over the solidified hook, which also entraps liquid mold flux and persists in the final microstructure. A hook tip that was fractured off, likely during liquid steel overflow, was revealed in the solidified microstructure, and explains the characteristic truncated shape of hook. Thus, the shape and size of hooks and oscillation marks are determined by two crucial events: (a) the curvature of the line of hook origin as dictated by the instantaneous shape of the meniscus during its solidification, and (b) the shape of the upper side of the oscillation mark, as dictated by the extent of liquid steel overflow.

A two-dimensional transient FE model has also been successfully used to reasonably predict shell shape and distortion due to a sudden level fluctuation event for ultralow-carbon steel slabs. A sudden level drop causes the shell tip to bend away from the mold due to thermal distortion. Subsequent rise in liquid level causes further shell bending. Shell thermal distortion is small for rapid level drops less than ±5 mm; however, for larger drops, such as 16 mm for 0.4 second, shell bending can be up to 0.46 mm for a 16-mm-long shell. Although shell thermal distortion alone cannot produce curved hooks and their associated oscillation marks, it is likely that shallower straight hooks, and the shape of the lower portion of other oscillation marks, can be explained by this mechanism. In particular, ultralow-carbon steels and peritectic steels, which tend to produce a stronger initial shell that cannot be flattened by ferrostatic pressure, can be expected to suffer more from this thermal distortion effect. This could help explain the increased oscillation mark depth experienced by these steels.

Acknowledgments

The authors wish to thank the Natural Sciences and Engineering Research Council of Canada, the National Science Foundation (Grant DMI-04-23794) and the Continuous Casting Consortium at the University of Illinois at Urbana-Champaign for support of this project.

References

1. Brimacombe, J.K., and Sorimachi, K., "Crack Formation in the Continuous Casting of Steel," *Metallurgical Transactions B,* 8B (1977), pp. 489–505.

2. Takeuchi, E., and Brimacombe, J.K., "The Formation of Oscillation Marks in the Continuous Casting of Steel Slabs," *Metallurgical Transactions B,* 15B (1984), pp. 493–509.

3. Takeuchi, E., and Brimacombe, J.K., "Effect of Oscillation ark Formation on the Surface Quality of Continuously Cast Steel Slabs," *Metallurgical Transactions B,* 16B (1985), pp. 605–625.

4. Yamamura, H., et al., "Formation of Solidified Hook-like Structure at the Subsurface in Ultralow-carbon Steel," *ISIJ International (Supplement),* 36 (1996), pp. S223–226.

5. Suzuki, M., "Initial Solidification Behaviour of Ultralow-carbon Steel," *CAMP-ISIJ,* 11 (1998), pp. 42–44.

6. Harada, S., et al., "A Formation Mechanism of Transverse Cracks on CC Slab Surface," *ISIJ International,* 30(4) (1990), pp. 310–316.

7. Shin, H-J., et al., "Effect of Mold Oscillation on Powder Consumption and Hook Formation in Ultralow-carbon Steel Slabs," *AISTech 2004 Iron & Steel Technology Conference Proceedings, Vol. II,* Association for Iron & Steel Technology (AIST), Warrendale, Pa., 2004, pp. 1157–1170.

8. Shin, H-J., et al., "Analysis of Hook Formation Mechanism in Ultralow-carbon Steel Using CON1D Heat Flow Solidification Model," *MS&T 2004 Conference Proceedings,* Association for Iron & Steel Technology (AIST) and TMS, Warrendale, Pa., 2004, pp. 11–26.

9. Genzano, C., et al., "Elimination of Surface Defects in Cold-rolled Extra Low Carbon Steel Sheet," *Iron & Steelmaker,* 29(6), June 2002, pp. 23–26.

10. Schmidt, K.D., et al., "Consequent Improvement of Surface Quality by Systematic Analysis of Slabs," *Steel Research International,* 74(11–12) (2003), pp. 659–666.

11. Birat, J-P., et al., "The Continuous Casting Mold: A Basic Tool for Surface Quality and Strand Productivity," *Steelmaking Conference Proceedings,* 74 (1991), pp. 39–40.

12. Emi, T., et al., "Influence of Physical and Chemical Properties of Mold Powders on the Solidification and Occurrence of Surface Defects of Strand Cast Slabs," *Proceedings of National Open Hearth and Basic Oxygen Steel Conference,* 61 (1978), pp. 350–361.

13. Schwerdtfeger, K., and Sha, H., "Depth of Oscillation Marks Forming in Continuous Casting of Steel," *Metallurgical and Materials Transactions B,* 31B (2000), pp. 813–826.

14. Saucedo, I.G., "Article Title Needed," *Steelmaking Conference Proceedings,* ISS-AIME, Warrendale, Pa., 1991, pp. 43–53.

15. Bo, K., et al., "Mechanism of Oscillation Mark Formation in Continuous Casting of Steel," *Journal of University of Science and Technology Beijing,* 7(3) (2000), pp. 189–192.

16. Putz, O., et al., "Investigations of Flow Conditions and Solidification in Continuous Casting Moulds by Advanced Simulation Techniques," *Steel Research,* 74(11–12) (2003), pp. 686–692.

17. Szekeres, E.S., "Overview of Mold Oscillation in Continuous Casting," *Iron and Steel Engineer,* 73(7) (1996), pp. 29–37.

18. Sato, R., "Powder Fluxes for Ingot Making and Continuous Casting," *Proceedings of National Open Hearth and Basic Oxygen Steel Conference,* AIME, Warrendale, Pa., 1979, pp. 48–67.

19. Savage, J., and Pritchard, W.H., "Problem of Rupture of Billet in Continuous Casting of Steel," *Iron and Steel,* 27(14) (1954), pp. 649–652.

20. Brendzy, J.L., et al., "Mould-strand Interaction in Continuous Casting of Steel Billets: Part 2. Lubrication and Oscillation Mark Formation," *Ironmaking and Steelmaking,* 20 (1) (1993), pp. 63–74.

21. Thomas, B.G., and Zhu, H., "Article Title Needed," *Proceedings of JIM/TMS Solidification Science and Processing Conference,* TMS, Warrendale, Pa., 1995, pp. 197–208.

22. Yamauchi, A., et al., "Cooling Behavior and Slab Surface Quality in Continuous Casting With Alloy 718 Mold," *ISIJ International,* 42(10) (2002), pp. 1094–1102.

23. Li, C., "Thermal-mechanical Model of Solidifying Steel Shell Behavior and Its Applications in High-speed Continuous Casting of Billets," Ph.D. thesis, University of Illinois at Urbana-Champaign, Urbana, Ill., 2004.

24. Voort, G.F.V., "Wetting Agents in Metallography," *Materials Characterization,* 35(2) (1995), pp. 135–137.

25. Sengupta, J., et al., "Micrograph Evidence of Meniscus Solidification and Subsurface Microstructure

Evolution in Continuous-cast Ultra-low Carbon Steels," *Acta Materialia,* 54(4) (2006), pp. 1165–1173.

26. Badri, A., et al., "A Mold Simulator for Continuous Casting of Steel: The Formation of Oscillation Marks During the Continuous Casting of Low-carbon Steel," *Metallurgical & Materials Transactions B,* 36B (2005), pp. 373–383.

27. Sengupta, J., and Thomas, B.G., "Effect of a Sudden Level Fluctuation on Hook Formation During Continuous Casting of Ultralow-carbon Steel Slabs," *Modeling of Casting, Welding, and Advanced Solidification Processes XI (MCWASP XI) Conference,* edited by C.Z. Gandin and J.E. Allision, Opio, France, May 28–June 2, 2006, pp. 727–236.

28. Meng, Y., and Thomas, B.G., "Article Title Needed," *Metallurgical Transactions B,* 34B (2003), pp. 685–705.

29. Lai, W., et al., "Article Title Needed," *83rd Steelmaking Conference Proceedings,* ISS-AIME, Warrendale, Pa., 2000, pp. 261–274.

30. Fredriksson, H., and Elfsberg, J., "Thoughts About the Initial Solidification Process During Continuous Casting of Steel," *Scandinavian Journal of Metallurgy,* 31 (2002), pp. 292–297.

31. Takeuchi, S., et al., "Control of Oscillation Mark Formation During Continuous Casting," *Steelmaking Conference Proceedings* (1991), pp. 37–41.

32. Lee, J., and Morita, K., "Evaluation of Surface Tension and Adsorption for Liquid Fe-S alloys," *ISIJ International,* 42(6) (2002), pp. 588–594.

33. Jimbo, I., and Cramb, A.W., "Calculations of the Effect of Chemistry and Geometry on Free Surface Curvature During Casting of Steels," *Iron & Steelmaker,* 20(6) (1993), pp. 55–63.

34. Sengupta, J., et al., "A Mew Mechanism of Hook Formation During Continuous Casting of Ultralow-Carbon Steel Slabs," *Metallurgical & Materials Transactions A,* 37A (5) (2006), pp. 1597–1611.

35. Tsutsumi, K., et al., "Inflow Behavior Observation of Molten Mold Powder Between Mold and Solidified Shell by Continuous Casting Simulator Using Sn-Pb Alloy and Stearic Acid," *ISIJ International,* 40 (2000), pp. 601–608.

36. Badri, A., et al., "A Mold Simulator for the Continuous Casting of Steel: The Development of a Simulator," *Metallurgical & Materials Transactions B,* 36B (2005), pp. 355–371. ✦

This paper was presented at AISTech 2006 — The Iron & Steel Technology Conference and Exposition, Cleveland, Ohio, and published in the AISTech 2006 Proceedings.